

N₂H⁺ and N¹⁵NH⁺ towards the prestellar core 16293E in L1689N

F. Daniel^{1,2}, A. Faure^{1,2}, L. Pagani³, F. Lique⁴, M. Gérin⁵, D. Lis^{3,6}, P. Hily-Blant^{1,2}, A. Bacmann^{1,2}, and E. Roueff⁷

¹ Univ. Grenoble Alpes, IPAG, F-38000 Grenoble, France

² CNRS, IPAG, F-38000 Grenoble, France

³ LERMA, Observatoire de Paris, PSL Research University, CNRS, Sorbonne Universités, UPMC Univ. Paris 06, F-75014, Paris, France

⁴ LOMC-UMR 6294, CNRS-Université du Havre, 25 rue Philippe Lebon, BP 1123 – 76063 Le Havre Cedex, France

⁵ LERMA, Observatoire de Paris, PSL Research University, CNRS, Sorbonne Universités, UPMC Univ. Paris 06, Ecole normale supérieure, F-75005, Paris, France

⁶ 301-17, California Institute of Technology, Pasadena, CA 91125, USA

⁷ LERMA, Observatoire de Paris, PSL Research University, CNRS, Sorbonne Universités, UPMC Univ. Paris 06, F-92190, Meudon, France

Received; accepted

ABSTRACT

Context. Understanding the processes that could lead to enrichment of molecules in ¹⁵N atoms is of particular interest in order to shed light on the relatively large variations observed in the ¹⁴N/¹⁵N ratio in various solar system environments.

Aims. Currently, the sample of molecular clouds where ¹⁴N/¹⁵N ratios have been measured is small and has to be enlarged in order to allow statistically significant studies. In particular, the N₂H⁺ molecule currently shows the largest spread of ¹⁴N/¹⁵N ratios in high-mass star forming regions. However, the ¹⁴N/¹⁵N ratio in N₂H⁺ was obtained in only two low-mass star forming regions (L1544 and B1b). The current work extends this sample to a third dark cloud.

Methods. We targeted the 16293E prestellar core, where the N¹⁵NH⁺ *J*=1-0 line was detected. Using a model previously developed for the physical structure of the source, we solved the molecular excitation with a non-local radiative transfer code. For that purpose, we computed specific collisional rate coefficients for the N¹⁵NH⁺-H₂ collisional system. As a first step of the analysis, the N₂H⁺ abundance profile was constrained by reproducing the N₂H⁺ *J*=1-0 and 3-2 maps. A scaling factor was then applied to this profile to match the N¹⁵NH⁺ *J*=1-0 spectrum.

Results. We derive a column density ratio N₂H⁺ / N¹⁵NH⁺ = 330⁺¹⁷⁰₋₁₀₀.

Conclusions. We performed a detailed analysis of the excitation of N₂H⁺ and N¹⁵NH⁺ towards the 16293E core, using state-of-the-art models to solve the radiative transfer, as well as the most accurate collisional rate coefficients available to date, for both isotopologues. We obtained the third estimate of the N₂H⁺ / N¹⁵NH⁺ column density ratio towards a cold prestellar core. The current estimate ~330 agrees with the value typical of the elemental isotopic ratio in the local ISM. It is however lower than in some other cores, where values as high as 1300 have been reported.

Key words. Astrochemistry — Radiative transfer — ISM: molecules — ISM: abundances

1. Introduction

Molecular isotopic ratios are invaluable tools for studying the origin of solar system materials and their possible link with interstellar chemistry. After hydrogen, the largest isotopic variations in the solar system are observed for nitrogen. The ¹⁴N/¹⁵N ratio varies by a factor of ~9, from the protosolar nebula (PSN) value of ~440 to the “hotspots” in meteorites where ratios as low as ~50 have been reported (see Füri & Marty 2015, and references therein). Enrichment in ¹⁵N with respect to the PSN value is observed in most objects of the solar system, except Jupiter. The reference value for cosmochemists is that of Earth with a ¹⁴N/¹⁵N ratio of 272 (measured in atmospheric N₂). In comets, the ¹⁴N/¹⁵N ratio has been measured in the three species : CN, HCN and NH₂, and the measurements were shown to cluster near ¹⁴N/¹⁵N~150 (see Rousselot et al. 2014, and references therein).

Several hypotheses have been proposed to explain ¹⁴N/¹⁵N enrichments in the solar system, which fall into two main categories. The first category concerns specific isotopic effects asso-

ciated with the N₂ photodissociation by UV light from the protosun or from nearby stars, such as self-shielding (Lyons et al. 2009, e.g.). In the second category, ¹⁵N enrichment is caused by chemical fractionation through ion-molecule reactions in the cold and dense interstellar medium (ISM), or in the cold regions of the protosolar disk.

In the dense ISM, direct observation of the nitrogen reservoir (presumably N or N₂) is not possible and the ¹⁴N/¹⁵N ratio has been obtained so far from the trace species N₂H⁺, NH₃, NH₂D, CN, HCN, and HNC. In the local ISM, ¹⁵N enrichments (¹⁴N/¹⁵N < 300) have been measured in CN, HCN and HNC (Ikeda et al. 2002; Adande & Ziurys 2012; Hily-Blant et al. 2013a; Wampfler et al. 2014), but not in the ammonia isotopologues for which the ¹⁴N/¹⁵N ratio is close to the PSN value or larger (Gerin et al. 2009; Lis et al. 2010; Daniel et al. 2013). The case of N₂H⁺ is the most intriguing, with values ranging from ~180 to ~1300 (Bizzocchi et al. 2013; Daniel et al. 2013; Fontani et al. 2015). The observational situation has thus significantly improved in the last five years, since

a number of new $^{14}\text{N}/^{15}\text{N}$ estimates have been made available. The results, however, are still puzzling. In fact, the large spread in molecular $^{14}\text{N}/^{15}\text{N}$ ratios reflects, at least partly, the difficulty of the measurements due to opacity and excitation effects, or the resort to the double isotope method. In addition, a gradient of $^{14}\text{N}/^{15}\text{N}$ with the galactocentric distance has been measured in CN and HNC by Amande & Ziurys (2012), as predicted by galactic chemical evolution models. The unambiguous observation of ^{15}N chemical fractionation in the ISM thus remains a challenging task. We also note that recently, the $^{14}\text{N}/^{15}\text{N}$ ratio has been determined for the first time in a protoplanetary disk (Guzmán et al. 2015). A ratio of 200 ± 100 was inferred from HCN, which is compatible with the measurements previously reported in dark clouds and comets.

Turning to theory, the pioneering model of Terzieva & Herbst (2000) predicted that chemical fractionation in ^{15}N should only be modest ($\sim 25\%$) and hardly detectable in the ISM. Subsequently, a fractionation mechanism based on CO depletion was suggested, predicting that two different pathways can drive the ^{15}N -fractionation: a slow one to ammonia and a rapid one to HCN and other nitriles (Charnley & Rodgers 2002; Rodgers & Charnley 2004, 2008). A chemical origin of the differential ^{15}N enrichment between hydrides and nitriles was also proposed by Hily-Blant et al. (2013a,b). In addition, by considering nuclear-spin effects in ion molecule reactions involving the ortho and para forms of H_2 , Wiström et al. (2012) have shown that the ^{15}N enrichments of nitriles do not correlate with deuterium (D) enrichments, as observed in meteorites. On the other hand, a recent reinvestigation of gas-phase chemical processes including D, ^{13}C and ^{15}N species has suggested that the main ^{15}N -fractionation routes are in fact inefficient (Roueff et al. 2015). Hence, though theory has improved, no model is currently able to reproduce the whole set of observational data. It is generally believed that important routes of nitrogen fractionation are still missing in the models (see, e.g., Fontani et al. 2015).

The dyazenilium ion (N_2H^+) is an interesting target for several reasons. First, chemically, it is a direct daughter product of N_2 , one of the two main nitrogen reservoirs with atomic nitrogen, through the proton transfer reaction $\text{N}_2 + \text{H}_3^+ \rightarrow \text{N}_2\text{H}^+ + \text{H}_2$. Second, the $^{14}\text{N}/^{15}\text{N}$ ratio in N_2H^+ can be determined without recourse to the double isotope method, a method commonly used for carbon bearing species (see, e.g., Amande & Ziurys 2012; Hily-Blant et al. 2013a,b). Third, accurate collisional rate coefficients for $\text{N}_2\text{H}^+ + \text{H}_2$ have recently been made available (see Lique et al. 2015, and below). Finally, observations of N_2H^+ show the largest variations in the $^{14}\text{N}/^{15}\text{N}$ ratio among all the nitrogen carriers. In the prestellar core L1544, this ratio was estimated as $\sim 1000 \pm 200$ (Bizzocchi et al. 2013) with N^{15}NH^+ and $^{15}\text{NNH}^+$ having nearly equal abundances. In the B1b molecular cloud, the $^{14}\text{N}/^{15}\text{N}$ ratio was estimated as 400^{+100}_{-65} in N^{15}NH^+ (Daniel et al. 2013). The low signal-to-noise ratio achieved for the observations of $^{15}\text{NNH}^+$ isotopologue led to a lower limit of 600 for this isotopologue. Finally, in high-mass star forming cores, the $^{14}\text{N}/^{15}\text{N}$ ratio was estimated in the range 180–1300 (Fontani et al. 2015).

In the present work, we provide a new measurement of the $^{14}\text{N}/^{15}\text{N}$ ratio derived from observations of two isotopologues of dyazenilium, N_2H^+ and N^{15}NH^+ , towards the low-mass prestellar core 16293E in L1689N. Note that contrary to the L1544 prestellar core, this source is not isolated and is influenced by the close-by Class 0 protostar IRAS 16293-2422. Towards this region, previous observations of some of the N_2H^+ isotopologues were reported by Castets et al. (2001) for N_2H^+ and Gerin et al.

(2001) for N_2D^+ . In Section 2, we give details on the observations used in this study. Section 3 describes the calculations performed for the $\text{N}^{15}\text{NH}^+ - \text{H}_2$ rate coefficients. Section 4 deals with the molecular excitation calculations and our conclusions are given in Section 5.

2. Observations

In the current study, we used the N_2H^+ $J=1-0$ SEST 15m telescope observations reported in Castets et al. (2001). We discovered, however, that these data suffered from observational artifacts, by comparing the observed spectra with spectra of the same line observed more recently at the IRAM 30m Telescope. This problem is further detailed below.

IRAM 30m observations of N_2H^+ were performed in early 2015 (17th of February and 2nd of April). Weather was bad, cloudy and unstable in February but excellent (1–2 mm precipitable water vapor) in April. Saturn, only a few degrees away from the source, was used for pointing and focusing of the telescope during both runs. Pointing was good with an uncertainty below $3''$. Observations were done with the EMIR0 receivers in frequency switch mode with both the autocorrelator (VESPA) at 9.8 kHz ($= 31.4 \text{ m s}^{-1}$) sampling and the fast fourier transform spectrometer (FFTS) at 48.8 kHz ($= 157 \text{ m s}^{-1}$) sampling. The rest frequency of the line for the main hyperfine component is 93173.764 MHz, following Pagani et al. (2009). T_{sys} was typically 100 K (T_a^* scale) with the source elevation ranging from 18.5° to 28.5° . Each integration lasted one minute and both polarisations were averaged and then folded. The typical noise is 70 mK (after subtracting a second or third order baseline). The FWHM beam size is $26.5''$ and the sampling was every $15''$. The main beam efficiency (0.80) is interpolated from an IRAM table (0.81 at 86 GHz and 0.78 at 115 GHz). These data will be presented and analysed in detail in a forthcoming paper (Pagani et al., in prep.) along with other observations.

Convolving the IRAM data to the SEST resolution, we find a relatively good correspondence in peak intensity, but not in the line profile. Consequently, the integrated intensity of the SEST data ($16.4 \pm 0.04 \text{ K km s}^{-1}$) is somewhat higher than the one from IRAM ($14.1 \pm 0.003 \text{ K km s}^{-1}$), i.e., +16%. The discrepancy is much larger than the systematic uncertainties. The SEST data (Castets et al. 2001) were obtained with an acousto-optical spectrometer which was the cause of an undue widening of the lines and line shape change, which cannot be reproduced by simply smoothing the IRAM data. To use the SEST data, we therefore multiplied them by 0.86 and introduced an ad-hoc convolution in frequency, as described in the next section.

Single-dish observations of the 1 mm molecular transitions presented here were carried out in 2013 May–June, using the 10.4 m Leighton Telescope of the Caltech Submillimeter Observatory (CSO) on Mauna Kea, Hawaii. We used the wide-band 230 GHz facility SIS receiver and the FFTS backend that covers the full 4 GHz intermediate frequency (IF) range with a 270 kHz channel spacing (0.37 km s^{-1} at 220 GHz). Pointing of the telescope was checked by performing five-point continuum scans of planets and strong dust continuum sources. The CSO main-beam efficiency at 230 GHz at the time of the observations was determined from total-power observations of planets to be $\sim 65\%$. The absolute calibration uncertainty is $\sim 15\%$ and the FWHM CSO beam size is $\sim 35''$ at 220 GHz.

The N^{15}NH^+ $J=1-0$ observations were performed in August 2014 with the IRAM-30m Telescope during average weather conditions (2–4 mm of precipitable water vapor). The Eight Mixer Receiver (EMIR) receiver was tuned to 92.0 GHz. We

used the FFTS backend with 49.8 kHz ($\sim 160 \text{ m s}^{-1}$) spectral resolution, leading to an instantaneous bandpass of 1.8 GHz and a velocity resolution of 0.16 km s^{-1} . The $J=1-0$ transition of $^{15}\text{NNH}^+$, around 90.25 GHz, was not covered with the chosen setup, which aimed at detecting other species. The system temperature was about 140 K and the source elevation varied between 18° and 28° . The observations were performed in position switching, with the reference position set $300''$ west of the source. The nearby planets Mars and Saturn were used for checking the telescope pointing and the focus. The data were reduced with CLASS and the noise level is 19 mK after removal of linear base lines.

3. N_2H^+ and N^{15}NH^+ collisional rate coefficients

Collisional rate coefficients for the $\text{N}_2\text{H}^+ - \text{H}_2(J=0)^1$ system have been published recently by Lique et al. (2015). Hyperfine-structure-resolved excitation rate coefficients, based on a new potential energy surface (PES) obtained from highly correlated *ab initio* calculations (Spielfiedel et al. 2015), were calculated for temperatures ranging from 5 K to 70 K. The new rate coefficients are significantly larger than the $\text{N}_2\text{H}^+ - \text{He}$ rate coefficients previously published (Daniel et al. 2005). In addition, the differences cannot be reproduced by a simple scaling relationship.

As a first approximation, these new rate coefficients could be used to analyse N^{15}NH^+ emission spectra since both N_2H^+ and N^{15}NH^+ share the same molecular properties (when the hyperfine splitting induced by the internal nitrogen is neglected). Recent studies, however, have shown that isotopic effects in inelastic collisions can be important (Scribano et al. 2010; Dumouchel et al. 2012), even in the case of $^{14}\text{N} \rightarrow ^{15}\text{N}$ substitution (Flower & Lique 2015). Hence, we have decided to compute specific $\text{N}^{15}\text{NH}^+ - \text{H}_2(J=0)$ rate coefficients.

Within the Born-Oppenheimer approximation, the full electronic ground state potential is identical for the $\text{N}_2\text{H}^+ - \text{H}_2$ and $\text{N}^{15}\text{NH}^+ - \text{H}_2$ systems and depends only on the mutual distances of the five atoms involved. Then, we used for the scattering calculations the $\text{N}_2\text{H}^+ - \text{H}_2$ PES of Spielfiedel et al. (2015) and the “adiabatic-hindered-rotor” treatment, which allows para- $\text{H}_2(J=0)$ to be treated as if it was spherical. Zero-point vibrational effects are different in N_2H^+ and N^{15}NH^+ , but these effects are expected to be moderate and are hence neglected in the present calculations. The only difference between the $\text{N}_2\text{H}^+ - \text{H}_2$ and $\text{N}^{15}\text{NH}^+ - \text{H}_2$ PES is thus the position of the center of mass taken for the origin of the Jacobi coordinates, an effect which has been taken into account in our calculations.

Since the ^{14}N and ^{15}N nitrogen atoms possess a non-zero nuclear spin ($I=1$ and $I=1/2$, respectively), the N_2H^+ and N^{15}NH^+ rotational energy levels are split into hyperfine levels. In the astronomical observations, however, the hyperfine structure due to ^{15}N is not resolved. The hyperfine levels of the N^{15}NH^+ molecules are thus characterized by the two quantum numbers J and F . Here, F results from the coupling of J with I (I being the nuclear spin of the external ^{14}N atom).

The hyperfine splitting in the N_2H^+ isotopologues is very small. Assuming that the hyperfine levels are degenerate, it is possible to simplify the hyperfine scattering problem using recoupling techniques as described in Daniel et al. (2004, 2005)

and in Faure & Lique (2012). Hence, we performed Close-Coupling calculations (Arthurs & Dalgarno 1960) for the pure rotational excitation cross-sections using the MOLSCAT program (Hutson & Green 1994), as in Lique et al. (2015) for the main isotopologue. The N^{15}NH^+ rotational energy levels were computed using the rotational constants of Dore et al. (2009). Calculations were carried out for total energies up to 500 cm^{-1} . Parameters of the integrator were tested and adjusted to ensure a typical precision to within 0.05 \AA^2 for the inelastic cross sections. At each energy, channels with J up to 28 were included in the rotational basis to converge the calculations for all the transitions between N^{15}NH^+ levels up to $J=7$. Using the recoupling technique and the stored S-matrix elements, the hyperfine-state-resolved cross-sections were obtained for all hyperfine levels up to $J=7$.

From the calculated cross-sections, one can obtain the corresponding thermal rate coefficients at temperature T by an average over the collision energy (E_c):

$$k_{\alpha \rightarrow \beta}(T) = \left(\frac{8}{\pi \mu k_B^3 T^3} \right)^{\frac{1}{2}} \times \int_0^\infty \sigma_{\alpha \rightarrow \beta}(E_c) E_c e^{-\frac{E_c}{k_B T}} dE_c \quad (1)$$

where $\sigma_{\alpha \rightarrow \beta}$ is the cross-section from initial level α to final level β , μ is the reduced mass of the system, and k_B is Boltzmann’s constant. Using the computational scheme described above, we have obtained $\text{N}^{15}\text{NH}^+ - \text{H}_2(J=0)$ rate coefficients for temperatures up to 70 K. These coefficients should have an accuracy similar to those computed for the main isotopologue by Lique et al. (2015). The main source of uncertainty is thus the use of the adiabatic-hindered-rotor approximation, which was shown to introduce errors below 5-10% (Lique et al. 2015; Spielfiedel et al. 2015). A typical accuracy of 10% is thus expected for the rate coefficients of the N_2H^+ isotopologues. The complete set of (de-)excitation rate coefficients with $J, J' \leq 7$ will be made available through the LAMDA (Schöier et al. 2005) and BASECOL (Dubernet et al. 2013) databases.

Figure 1 presents the temperature variation of the $\text{N}_2\text{H}^+ - \text{H}_2(J=0)$ and $\text{N}^{15}\text{NH}^+ - \text{H}_2(J=0)$ rate coefficients for a few hyperfine transitions associated with the $J=3 \rightarrow 2$ and $2 \rightarrow 1$ rotational transitions. To enable a direct comparison, we summed the $\text{N}_2\text{H}^+ - \text{H}_2(J=0)$ rate coefficients over the hyperfine structure associated with the internal nitrogen nucleus. As one can see, the differences between the N_2H^+ and N^{15}NH^+ rate coefficients are moderate. The two sets of data differ by less than 20 percent over the whole temperature range. We find, however, that the largest deviations occur at temperatures typical of cold molecular clouds ($T=5-20 \text{ K}$) and we observe that the N_2H^+ over N^{15}NH^+ rate coefficients ratios tend to increase with decreasing temperature. The differences are due to both the centre-of-mass shift in the interaction potential and the use of a specific description of the isotopologue energy levels. In conclusion, we found that the isotopologue specific results differed from each other to an extent that they may be significant for analyses of observations of the hyperfine transitions of these species, at least for cold dark cloud conditions. Modeling N^{15}NH^+ with N_2H^+ rate coefficients will typically induce errors in the N^{15}NH^+ column density estimate of the same order of magnitude as the differences found in rate coefficients. Hence, we can expect that earlier studies that resorted to the same set of rates for both isotopologues would not suffer from errors larger than 20%. In particular, we expect this conclusion to remain true in the case where He is the collisional partner (Daniel et al. 2005).

¹ In molecular dynamics, the rotational quantum numbers are noted j , and J refers to the total angular momentum. However, in what follows, we use the spectroscopic notation and denote the rotational quantum number as J . This choice is made for consistency with the other parts of the article since the spectroscopist notation is usually adopted in astrophysical studies.

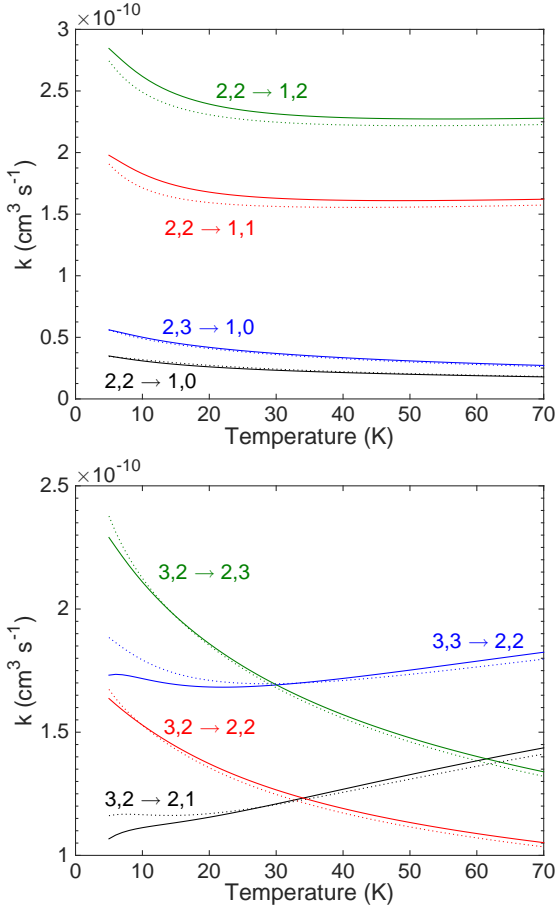


Fig. 1: Temperature variation of the hyperfine resolved $\text{N}_2\text{H}^+ - \text{H}_2(j=0)$ (solid lines) and $\text{N}^{15}\text{NH}^+ - \text{H}_2(j=0)$ (dotted lines) rate coefficients for $j = 2, F \rightarrow j' = 1, F'$ and $j = 3, F \rightarrow j' = 2, F'$ transitions.

4. Radiative transfer modeling

To obtain an accurate estimate of the $^{14}\text{N}/^{15}\text{N}$ ratio in N_2H^+ , we obtained the column densities of the two isotopologues by solving the molecular excitation problem. The methodology used is similar to the approach described in Daniel et al. (2013), where the $^{14}\text{N}/^{15}\text{N}$ ratio was estimated for various molecules towards B1b. In the present case, our analysis deals with the 16293E prestellar core. To perform the analysis, we have used the physical structure of 16293E described in Bacmann et al. (2016). In that study, variations of the H_2 density and dust/gas temperature throughout the core were derived using continuum observations at wavelengths ranging from $160\ \mu\text{m}$ to $1.3\ \text{mm}$. The core center was then fixed at an intermediate distance between the maxima of the $850\ \mu\text{m}$ and $1.3\ \text{mm}$ maps. More precisely, its coordinates are fixed at $\alpha = 16^{\text{h}}32^{\text{m}}28.8^{\text{s}}$, $\delta = -24^{\circ}29'4''$ (J2000). In what follows, the offsets indicated in the figures are given according to this reference position.

The N_2H^+ spectroscopy is taken from Caselli et al. (1995) and Pagani et al. (2009). For the main N_2H^+ isotopologue, the $\text{N}_2\text{H}^+ - \text{H}_2$ rate coefficients are taken from Lique et al. (2015). For the rare N^{15}NH^+ isotopologue, the rate coefficients were described in the previous section and the spectroscopy is taken from Dore et al. (2009). Finally, the molecular excitation and radiative transfer are solved with the 1Dart code described in Daniel & Cernicharo (2008), which takes into account the line

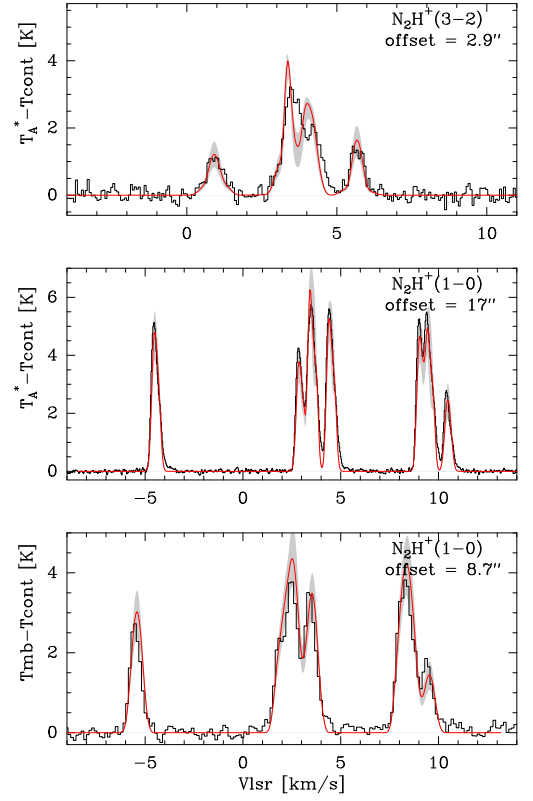


Fig. 2: Comparison between model and observations for the SEST (bottom panel) and IRAM (middle panel) $\text{N}_2\text{H}^+ J=1-0$ line. The top panel shows the CSO $\text{N}_2\text{H}^+ J=3-2$ line. In each panel, we give the offset between the position observed and the core center. For each spectrum, the grey area indicates the variation of intensity obtained by varying the N_2H^+ abundance as is indicated in Fig. 5

overlap between hyperfine lines.

As a first step of our analysis, we constrained the abundance of the main N_2H^+ isotopologue throughout the core. To that purpose, we made use of the $J=1-0$ and $J=3-2$ maps, respectively observed at the SEST and CSO telescopes. Additionally, we used a spectrum of the $J=1-0$ line, observed at the IRAM 30m Telescope towards a position offset by $\sim 17''$ from the core center. The comparison between the IRAM and SEST observations made by degrading the IRAM data to the SEST resolution show that the spectra obtained at the SEST telescope have broader linewidths (see Section 2). To explain these differences, we assumed that the SEST observations suffered from systematic uncertainties and we thus only took into account the relative variations of the spectra from one map position to another. Additionally, to reproduce the observational artifact linked to the SEST observations, we performed a spectral convolution of the synthetic spectra, with a spectral response given by a Gaussian. The associated width was adjusted so that a model that would fit the IRAM 30m $J=1-0$ spectra would give an equally good fit for the closest SEST observation. The corresponding point of the SEST map is $8.7''$ from the core center and the IRAM 30m and SEST $J=1-0$ observations are distant by $\sim 10''$ from each other. The result of this procedure corresponds to the observations plotted in the bottom and middle panels of Fig. 2.

As previously said, the modeling is performed using the physical structure (i.e., H_2 density, gas and dust temperatures, ...) described in Bacmann et al. (2016). As a reminder, the density is constant at $\sim 1.4 \times 10^7 \text{ cm}^{-3}$ within a radius of $4''$ and then decreases outward. The temperature at the core center is 11 K and increases outwards up to 16 K. The only free parameters of the current modeling are thus linked to the N_2H^+ abundance profile. To fit the observations, we introduced radial zones within which the N_2H^+ abundance is kept constant. We started with the simplest model, i.e., with a constant abundance throughout the cloud (i.e. one free parameter). We then increased the number of radial zones, i.e., the number of free parameters, until we obtained a reasonable fit to the observations, the quality of the fit being gauged by eye. Doing so, a satisfactory fit is obtained with only three radial regions. The fit of the $J=1-0$ and $3-2$ lines obtained at positions close to the core center are shown in Fig. 2, and the SEST and CSO maps are shown in Fig. 3 and Fig. 4. As can be seen in these Figures, some discrepancies exist between the model and observations at some particular positions. We estimate, however, that the overall agreement is satisfactory given the non-sphericity of the 16293E core (see the molecular emission maps in, e.g., Castets et al. 2001; Lis et al. 2002). The N_2H^+ abundance that corresponds to these observations is reported in Fig. 5. In each region of the abundance profile, we determined error bars by varying the N_2H^+ abundance so that the resulting spectra did not depart significantly from the best model. The corresponding variations from our best estimate correspond to the grey zones in Fig. 2. The column density inferred from this model towards the center of the sphere is $N(\text{N}_2\text{H}^+) = 4.6^{+6.0}_{-1.2} 10^{13} \text{ cm}^{-2}$.

To model the spectrum of the N^{15}NH^+ $J=1-0$ line observed at $\sim 15''$ from the core center, we assumed that the abundance profile is similar to that of the main isotopologue. The observed spectrum is then reproduced by introducing an overall scaling factor to the abundance. The observations are correctly reproduced with an abundance ratio $\text{N}_2\text{H}^+ / \text{N}^{15}\text{NH}^+ \sim 330^{+170}_{-100}$ and the comparison between the model and observations is shown in Fig. 6. In this Figure, the grey area corresponds to the error bars of the ratio.

As in Daniel et al. (2013), we can calculate a mean excitation temperature \bar{T}_{ex} from the source model. For the N_2H^+ and N^{15}NH^+ $J=1-0$ lines, we respectively derive values of $9.44^{+0.97}_{-1.13}$ K and $9.48^{+0.01}_{-0.01}$ K, where the sub- and superscripts indicate the spread of values over all the hyperfine components. The larger spread of values for the main isotopologue is a consequence of larger line opacities which is accompanied by a departure from a single excitation temperature (Daniel et al. 2006). The opacities summed over all the components are respectively ~ 17.3 and 0.06 for the N_2H^+ and N^{15}NH^+ isotopologues. Note that despite the higher opacity of the N_2H^+ $J=1-0$ line, \bar{T}_{ex} is not enhanced by line trapping effects for this isotopologue. In fact, in the current case, the increase in T_{ex} due to line trapping is counterbalanced by the increase of the $\text{N}^{15}\text{NH}^+ - \text{H}_2$ rate coefficients. Indeed, in the model of B1b, Daniel et al. (2013) found that the \bar{T}_{ex} of N_2H^+ was enhanced by $\sim 17\%$ with respect to the N^{15}NH^+ \bar{T}_{ex} , the two calculations being performed with the same set of rate coefficients. Hence, in the current case, the assumption of a similar T_{ex} to describe the two isotopologues would apply.

5. Discussion

As explained in the Introduction, the large variations of the $^{14}\text{N}/^{15}\text{N}$ ratio in the solar system are not understood. As a re-

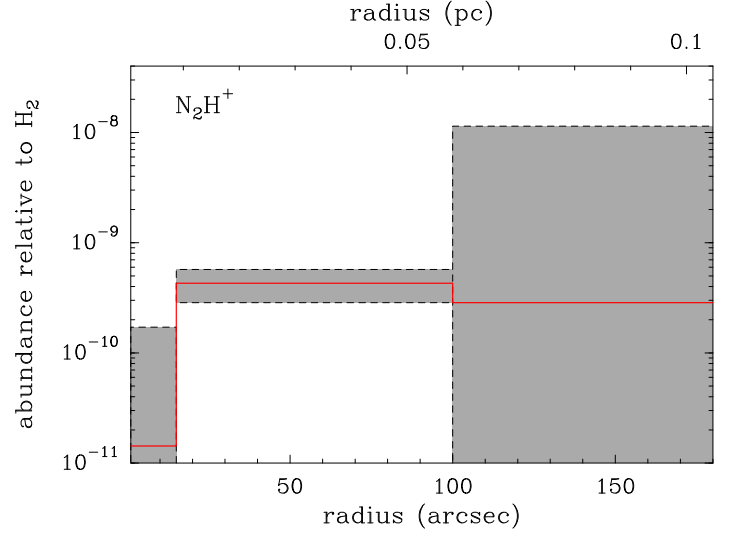


Fig. 5: N_2H^+ abundance profile.

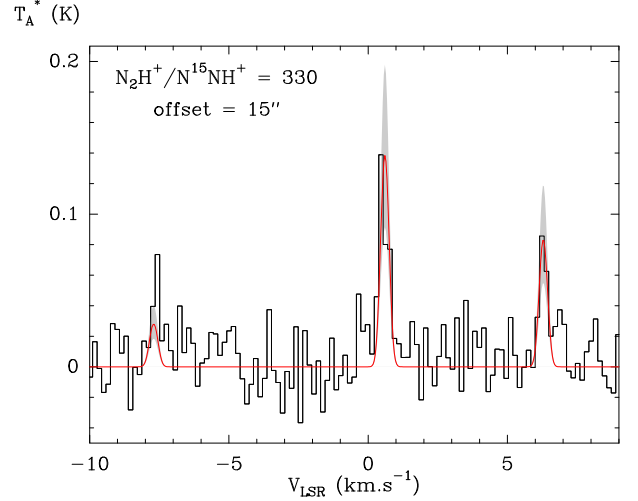


Fig. 6: Comparison between model and observations for the N^{15}NH^+ $J=1-0$ line.

minder, this ratio is ~ 440 in the solar wind, ~ 270 on Earth, and ~ 150 in comets. We refer the reader to Füre & Marty (2015) for a recent review of the literature. The main question is whether the ^{15}N enrichments indicate interstellar inheritance, nitrogen fractionation in the protoplanetary disk phase, or both. Guzmán et al. (2015) showed recently that the average $^{14}\text{N}/^{15}\text{N}$ ratio in HCN towards the MWC 480 disk is 200 ± 100 . This value is comparable to the ratios observed in comets and in dark clouds, but the signal-to-noise ratios of those data was not high enough to allow a pre-stellar or protoplanetary disk origin to be distinguished (see the discussion in Guzmán et al. 2015). In addition, as explained above, ^{15}N enrichments derived in HCN are ambiguous due to the possible depletion of ^{13}C (Roueff et al. 2015).

In the present work, we have provided a new measurement of the $^{14}\text{N}/^{15}\text{N}$ ratio in a prestellar core by observing N_2H^+ and N^{15}NH^+ . The derived abundance ratio $\text{N}_2\text{H}^+ / \text{N}^{15}\text{NH}^+ \sim 330^{+170}_{-100}$ is comparable to the elemental isotope ratio inferred for the local ISM, which is estimated as $^{14}\text{N}/^{15}\text{N} = 290 \pm 40$ by Amande & Ziurys (2012), from a survey of CN and HCN rotational lines. More recently, Ritchey et al. (2015) derived a lo-

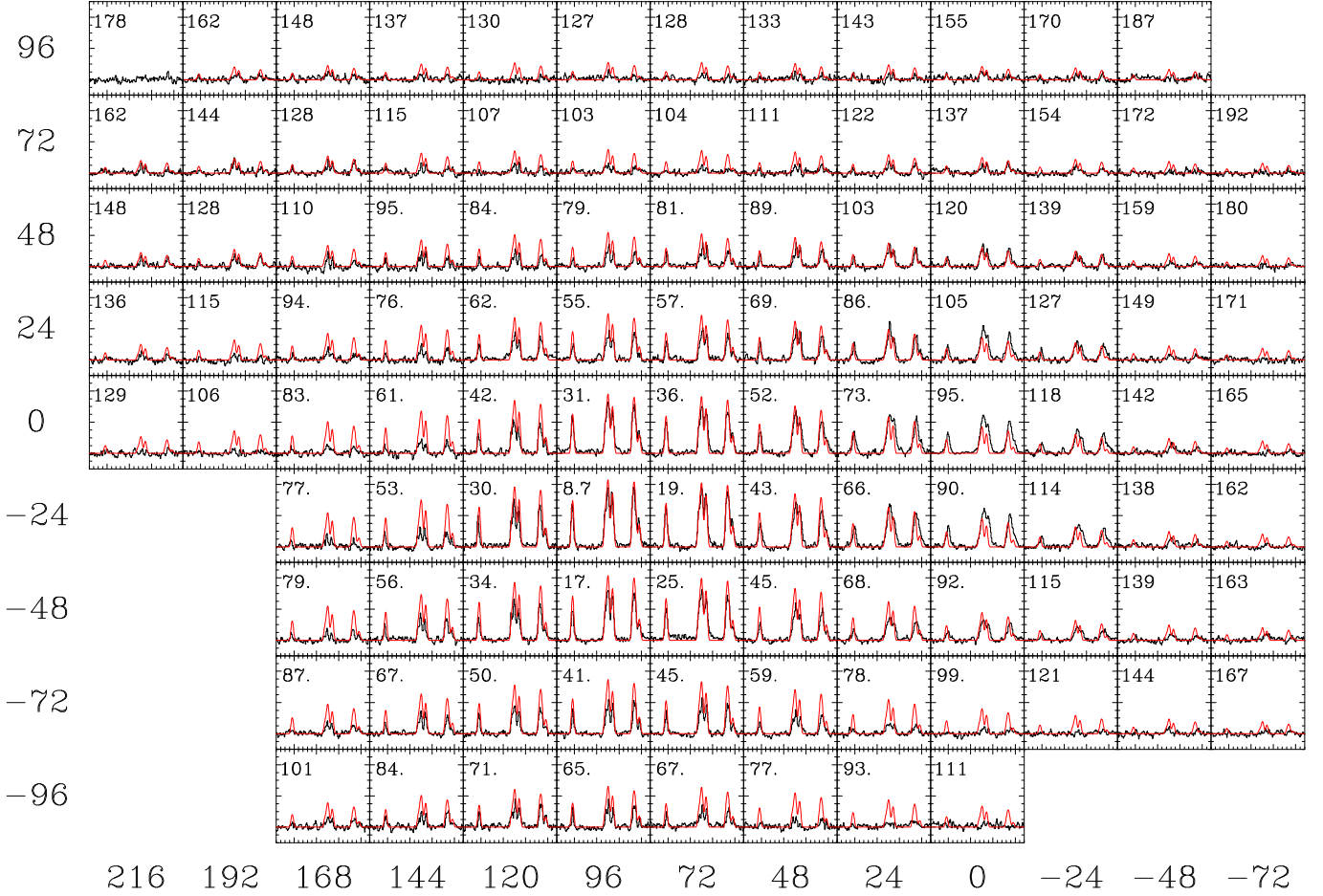


Fig. 3: Comparison between model and observations for the $\text{N}_2\text{H}^+(J=1-0)$ map observed at SEST. In each panel, the distance to the core center is indicated, in arcseconds, in the upper left side of the box. The reference coordinates of the map is $\alpha = 16^{\text{h}}32^{\text{m}}22.76^{\text{s}}$, $\delta = -24^{\circ}28'33.1''$ (J2000), as given in Castets et al. (2001), which corresponds to a position close to the 16293-2422 protostar. This protostar is at $\sim 90''$ at the North–West of the 16293E core center.

cal ISM value $^{14}\text{N}/^{15}\text{N} = 274 \pm 18$ from UV absorption lines of CN towards four lines of sight. Given the error bars, a ratio of ~ 300 would apply to the 16293E region. This similarity to local ISM values would imply an absence of chemical fractionation for N_2H^+ in this source, in dense gas. Indeed, the most recent gas-phase network of Roueff et al. (2015) suggests that the fractionation reaction of ^{15}N with N_2H^+ is inefficient due to the presence of an activation barrier, in contrast to the hypothesis made in previous models. In particular, the network of Hily-Blant et al. (2013b) does predict ^{15}N enrichment in N_2H^+ , in very good agreement with the present observation, but assumes a solar elemental ratio of 440. An $^{14}\text{N}/^{15}\text{N}$ value of ~ 300 , however, might be more appropriate to describe the local ISM. In that case, the difference with the PSN value then would be a consequence of the stellar nucleosynthesis that enriched the ISM in ^{15}N atoms by $\sim 50\%$, during the last 4.5 Gy (Ritchey et al. 2015).

More observations are clearly needed to establish the actual elemental ratio in 16293E and to confirm or exclude nitrogen chemical fractionation in N_2H^+ . In particular, observing various ^{15}N -substituted molecules is important since it would allow us to disentangle between fractionation effects or a variation of the elemental abundance ratio from the mean local ISM value. Indeed, in the first case, we expect to obtain a spread in the ratios, while in the second case, all the isotopic ratios should cluster around the same value.

More generally, it should be noted that gas-phase models of chemical fractionation are dependent on the temperature, on the chosen elemental abundances (especially the C/O ratio) and on the ortho-to-para ratio of H_2 (Hily-Blant et al. 2013b; Le Gal et al. 2014; Roueff et al. 2015). It is also crucial to couple C, N and O isotopic chemistries, as emphasized by Roueff et al. (2015). As a result, small variations in chemical conditions can have a strong impact on the predicted molecular $^{14}\text{N}/^{15}\text{N}$ ratios. We note in this context that the temperature at the core center is higher in 16293E (~ 11 K), where $\text{N}_2\text{H}^+ / \text{N}^{15}\text{NH}^+ \sim 330$, than in L1544 (~ 6 K), where $\text{N}_2\text{H}^+ / \text{N}^{15}\text{NH}^+ \sim 1000$. It is unclear whether such a small temperature difference can play a role but this should be investigated in detail in future dedicated studies. The large spread observed in high-mass star forming regions reported by Fontani et al. (2015) ($\text{N}_2\text{H}^+ / \text{N}^{15}\text{NH}^+ \sim 180-1300$) could also reflect temperature or elemental abundance effects. It could also be partly due to the gradient of the $^{14}\text{N}/^{15}\text{N}$ abundance ratio with galactocentric distance (Adande & Ziurys 2012). In any case, the statistics of objects with a determination of the $^{14}\text{N}/^{15}\text{N}$ ratio in various molecules has to be enlarged if we want to answer the question of the origin of nitrogen fractionation in the solar system.

Acknowledgements. This work has been supported by the Agence Nationale de la Recherche (ANR-HYDRIDES), contract ANR-12-BS05-0011-01 and by the CNRS national program “Physico-Chimie du Milieu Interstellaire”. This work

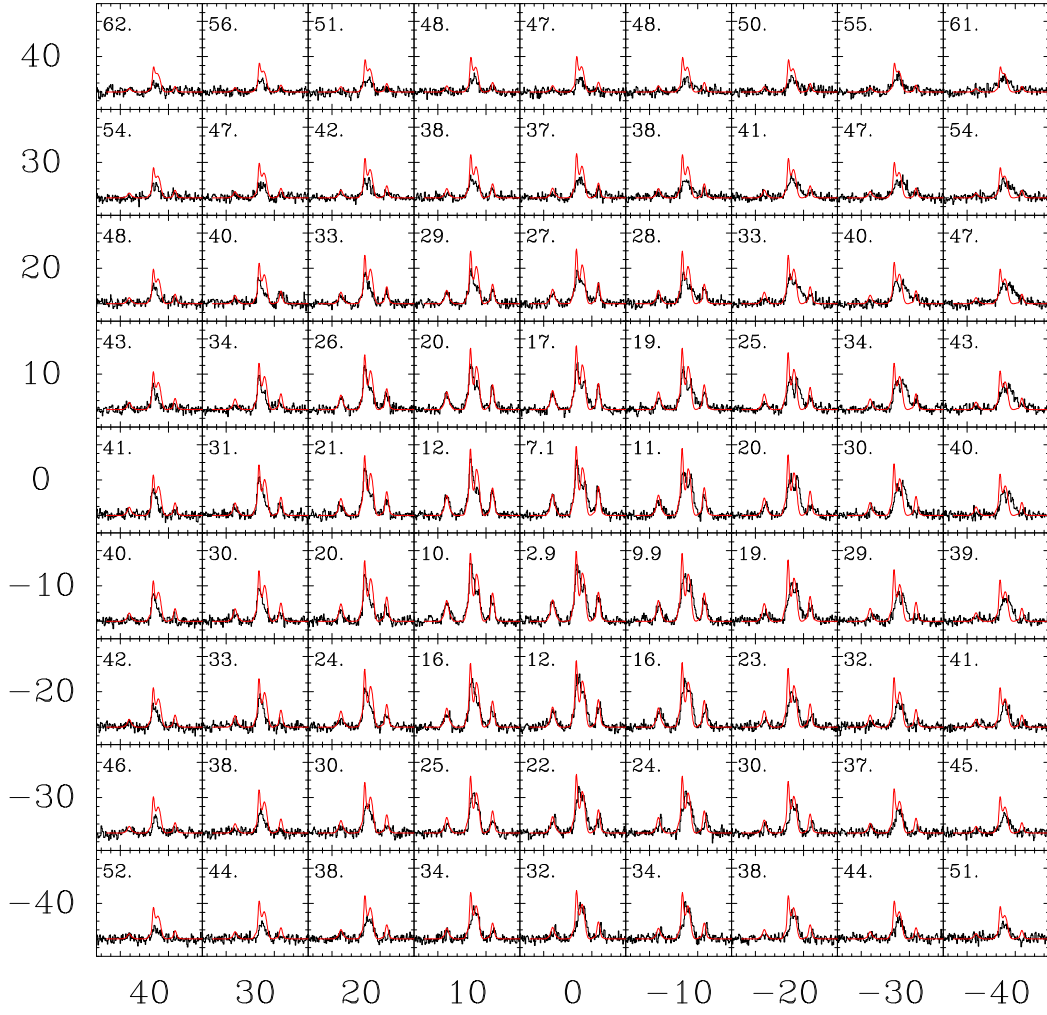


Fig. 4: Comparison between model and observations for the N_2H^+ ($J=3-2$) map observed at CSO. In each panel, the distance to the core center is indicated, in arcseconds, in the upper left side of the box. The reference coordinates of the map is $\alpha = 16^{\text{h}}32^{\text{m}}28.83^{\text{s}}$, $\delta = -24^{\circ}28'56.9''$ (J2000), which is at $\sim 7''$ from the position we assume for the core center.

is based upon observations with the the Caltech Submillimeter Observatory, operated by the California Institute of Technology. Support for this work was provided by NASA through an award issued by JPL/Caltech. The authors thank A. Castets for providing the N_2H^+ data acquired with the SEST telescope.

References

- Adande, G. R. & Ziurys, L. M. 2012, *ApJ*, 744, 194
- Arthurs, A. M. & Dalgarno, A. 1960, *Proc. R. Soc. London, Ser. A*, 256, 540
- Bacmann, A., Daniel, F., Caselli, P., et al. 2016, *A&A*, 587, A26
- Bizzocchi, L., Caselli, P., Leonardo, E., & Dore, L. 2013, *A&A*, 555, A109
- Caselli, P., Myers, P. C., & Thaddeus, P. 1995, *ApJ*, 455, L77
- Castets, A., Ceccarelli, C., Loinard, L., Caux, E., & Lefloch, B. 2001, *A&A*, 375, 40
- Charnley, S. B. & Rodgers, S. D. 2002, *ApJ*, 569, L133
- Daniel, F. & Cernicharo, J. 2008, *A&A*, 488, 1237
- Daniel, F., Cernicharo, J., & Dubernet, M.-L. 2006, *ApJ*, 648, 461
- Daniel, F., Dubernet, M.-L., & Meuwly, M. 2004, *J. Chem. Phys.*, 121, 4540
- Daniel, F., Dubernet, M.-L., Meuwly, M., Cernicharo, J., & Pagani, L. 2005, *MNRAS*, 363, 1083
- Daniel, F., Gérin, M., Roueff, E., et al. 2013, *A&A*, 560, A3
- Dore, L., Bizzocchi, L., Degli Esposti, C., & Tinti, F. 2009, *A&A*, 496, 275
- Dubernet, M.-L., Alexander, M. H., Ba, Y. A., et al. 2013, *A&A*, 553, A50
- Dumouchel, F., Klos, J., Toboła, R., et al. 2012, *J. Chem. Phys.*, 137, 114306
- Faure, A. & Lique, F. 2012, *MNRAS*, 425, 740
- Flower, D. R. & Lique, F. 2015, *MNRAS*, 446, 1750
- Fontani, F., Caselli, P., Palau, A., Bizzocchi, L., & Ceccarelli, C. 2015, *ApJ*, 808, L46
- Füri, E. & Marty, B. 2015, *Nature Geoscience*, 8, 515
- Gerin, M., Marcelino, N., Biver, N., et al. 2009, *A&A*, 498, L9
- Gerin, M., Pearson, J. C., Roueff, E., Falgarone, E., & Phillips, T. G. 2001, *ApJ*, 551, L193
- Guzmán, V. V., Öberg, K. I., Loomis, R., & Qi, C. 2015, *ApJ*, 814, 53
- Hily-Blant, P., Bonal, L., Faure, A., & Quirico, E. 2013a, *Icarus*, 223, 582
- Hily-Blant, P., Pineau des Forêts, G., Faure, A., Le Gal, R., & Padovani, M. 2013b, *A&A*, 557, A65
- Hutson, J. M. & Green, S. 1994, *MOLSCAT* computer code, version 14 (1994), distributed by Collaborative Computational Project No. 6 of the Engineering and Physical Sciences Research Council (UK)
- Ikeda, M., Hirota, T., & Yamamoto, S. 2002, *ApJ*, 575, 250
- Le Gal, R., Hily-Blant, P., Faure, A., et al. 2014, *A&A*, 562, A83
- Lique, F., Daniel, F., Pagani, L., & Feautrier, N. 2015, *MNRAS*, 446, 1245
- Lis, D. C., Gerin, M., Phillips, T. G., & Motte, F. 2002, *ApJ*, 569, 322
- Lis, D. C., Wootten, A., Gerin, M., & Roueff, E. 2010, *ApJ*, 710, L49
- Lyons, J. R., Bergin, E. A., Ciesla, F. J., et al. 2009, *Geochim. Cosmochim. Acta*, 73, 4998
- Pagani, L., Daniel, F., & Dubernet, M.-L. 2009, *A&A*, 494, 719
- Ritchey, A. M., Federman, S. R., & Lambert, D. L. 2015, *ApJ*, 804, L3
- Rodgers, S. D. & Charnley, S. B. 2004, *MNRAS*, 352, 600
- Rodgers, S. D. & Charnley, S. B. 2008, *ApJ*, 689, 1448
- Roueff, E., Loison, J. C., & Hickson, K. M. 2015, *A&A*, 576, A99
- Rousselot, P., Pirali, O., Jehin, E., et al. 2014, *ApJ*, 780, L17
- Schöier, F. L., van der Tak, F. F. S., van Dishoeck, E. F., & Black, J. H. 2005, *A&A*, 432, 369
- Scribano, Y., Faure, A., & Wiesenfeld, L. 2010, *J. Chem. Phys.*, 133, 231105

- Spielfiedel, A., Senent, M. L., Kalugina, Y., et al. 2015, J. Chem. Phys., 143, 024301
- Terzieva, R. & Herbst, E. 2000, MNRAS, 317, 563
- Wampfler, S. F., Jørgensen, J. K., Bizzarro, M., & Bisschop, S. E. 2014, A&A, 572, A24
- Wirström, E. S., Charnley, S. B., Cordiner, M. A., & Milam, S. N. 2012, ApJ, 757, L11